TRANSIENT MODELING OF IMPINGING HEAT TRANSFER FROM AN ACOUSTICALLY MODULATED TURBULENT AIR JET TO A NORMALLY POSITIONED FLAT SURFACE

by

Dejan B. CVETINOVIĆ[a*], Nikola M. ĆETENOVIĆ[a], Aleksandar M. ERIĆ[a], Jovana D. ANDJELKOVIĆ[a], and Djordje S. ČANTRAK[b]

[a]Laboratory for Thermal Engineering and Energy, "Vinča" Institute of Nuclear Sciences, National Institute of the Republic of Serbia, University of Belgrade, Belgrade, Serbia
[b]Faculty of Mechanical Engineering, University of Belgrade, Belgrade, Serbia

Original scientific paper
https://doi.org/10.2298/TSCI2501767C

The subject of this study is the numerical investigation of the impingement of an axisymmetric turbulent air jet on a flat surface, the influence of acoustic modulations on the coherent structures that form around the jet, and the effects on the heat transfer from the jet to the heated surface. The study showed how controlled acoustic perturbations influence the exit velocity profile from the nozzle and the formation of vortices in the boundary-layer of the jet. Since vortices are responsible for the redistribution of thermal energy transferred from the jet to the surface in impinging jet flow configurations, it is crucial to investigate whether their formation and evolution can be controlled. The results of the numerical simulations indicated very good agreement with experimentally measured velocity field. However, a problem arises in the prediction of the heat transfer because the standard k-ε model overestimates the values of the heat transfer coefficient in the stagnation zone because they were theoretically developed to use shear stresses for the generation of the turbulent kinetic energy, while in reality normal stresses are responsible for their generation in this flow situation. Due to the unstructured mesh used for the calculations, there are discrepancies in the results at larger edge distances. The complex flow at the impingement surface, the occurrence of secondary vortices and re-circulation zones and their direct effect on the heat transfer cannot be fully captured by the mathematical model, even if the numerical errors are acceptable compared to experiments.

Key words: *turbulent axisymmetric air jet, vortex structures, numerical investigations, heat transfer*

Introduction

The methodology described in this work finds application in the cooling of turbomachinery (gas turbine blades), combustion chambers, heat exchangers, electronic components cooling, paper drying processes, welding machines, *etc*. The heat transfer coefficient, which is of interest here, is a complex function of multiple parameters: Reynolds number, Prandtl number, dimensionless distance from the nozzle to the impact surface, *L/D*,

*Corresponding author, e-mail: deki@vin.bg.ac.rs

dimensionless radial distance from the stagnation point along the impact surface, *r/D*, nozzle geometry, turbulence, and energy redistribution in the jet. Variable *D* represents inner diameter of nozzle [1-4].

Acoustic waves can induce disturbances in the boundary-layer and vortex formation at the periphery of the jet exiting the nozzle, thus affecting the exit velocity profile from the nozzle. Vortices are responsible for redistributing the thermal energy transferred from the heated surface to the jet, hence it is of interest to establish whether their formation and development can be controlled.

All of this will be investigated from a numerical perspective using simulations [5], while experiments conducted by [6, 7], will serve as a relevant database for comparison. The software package to be used for numerical simulations is ANSYS FLUENT, where results obtained based on turbulent mathematical models implemented within the program, will be presented. In the examined case, there is flow that is normal to the impinging plate, which then transitions into flow parallel to the impinging plate. Mathematical models can accurately predict the physics of the problem at larger radial distances from the jet axis, but they err in predicting heat transfer at the stagnation zone because they use shear stresses to generate turbulent kinetic energy, whereas normal stresses are responsible for this phenomenon in reality. In the case under consideration, the working fluid is air-air.

The fluid-flow during its movement can be divided into three zones: the free jet region consisting of the potential core and the boundary-layer, the stagnation zone where the fluid impacts the impinging plate and the region of fluid movement along the impinging plate. In the potential core, which extends axially for several diameters of the nozzle, the fluid is identical to that exiting the nozzle, and once this core is disrupted at 6-7 diameters, *D*, of axial distance, developed turbulence occurs. The boundary-layer is at the periphery of the jet and consists of vortices that grow over time, causing the jet to expand and eventually penetrate to the axis of the jet, disrupting the potential flow. The boundary-layer depends on the nozzle shape and it determines forming of vortices at the fluid-material interface at the nozzle exit. Upon leaving the nozzle, vortices develop at the location of the boundary-layer. The stagnation zone is characterized by a high pressure gradient because the fluid loses speed and turbulence but gains pressure there, driving its further movement along the impinging plate. As the fluid moves radially along the impinging plate, it increases in velocity, thereby maintaining a thin boundary-layer, which facilitates a higher heat transfer rate at these locations. As the fluid moves along the impinging plate, it gradually slows down over time, leading to the expansion of the jet and an increase in the boundary-layer thickness, resulting in a decrease in the heat transfer coefficient.

Theoretical assumptions

When observing a jet with impingement on a impinging plate and its characteristics near the nozzle, no significant differences are observed compared to the properties of a free jet without the presence of a impinging plate. Essential characteristics by which the properties of the jet upon exiting the nozzle are described include: the initial thickness of the spreading layer at the nozzle exit, δ, and the diameter, *D*. The ratio of δ and *D* represents a shape factor, *H*, from which it can be inferred whether laminar or turbulent flow is occurring.

Shearing layers are inherently unstable, so disturbance waves lead to the formation of vortices. Therefore, disturbances of any nature (*e.g.*, acoustic) behave in the form of waves, and for this reason, they can be represented in the form of the dimensionless Strouhal, S_{tD}, number. In its downstream flow, vortices can pair up, resulting in a larger vortex. It may occur that more

than two vortices interact, but for their stable pairing to occur, the excitation frequency needs to be the first, second, or third subharmonic of the natural frequency of the vortex. [8]

As vortices develop, the flow transitions to complete turbulence, and the shearing layer begins to occupy space closer to the jet axis at larger axial distances. Various experiments have been conducted by numerous authors, demonstrating certain dependencies between excitation (S_{tD}, where D refers to the diameter of the nozzle) and the velocity field and turbulence in the jet [2, 3, 6, 7]. It has been established that at $S_{tD} = 0.3$, considered the desired excitation mode, there is a faster transition to turbulence, the spreading layer penetrates to the jet axis more rapidly, and the potential core is shorter. Due to vortex development, turbulence intensity peaks occur at specific axial distances from the nozzle, and when compared to other excitations, these peaks are the highest. At this excitation, vortex pairing does not occur, which instead happens at an excitation frequency corresponding to $S_{tD} = 0.6$. At slightly higher Strouhal numbers (around 1), vortices exhibit completely unpredictable motion, and turbulence peaks can be observed very close to the jet axis at short axial distances. When $S_{tD} = 2$, turbulence intensity is lower than in previous cases and more uniform, but this excitation can only be achieved in the form of external excitation (loudspeaker). Reynolds number, Strouhal number, and excitation intensity are essential factors influencing the behavior of the free jet.

A crucial interaction occurs between vortices and the impinging plate, determining whether boundary-layer separation occurs. This is important due to heat transfer from the impinging plate to the air. Unsteady boundary-layer separation can occur in both excited and unexcited jets if the axial distance between the impinging plate and the nozzle is too small. In such cases, vortices do not develop sufficiently, and with a large negative pressure gradient, they reach the impinging plate layer. The primary vortex, with such a gradient, upon reaching the impinging plate, accelerates the fluid outside the boundary-layer while decelerating the fluid within the boundary-layer. Consequently, a spreading layer forms between the boundary-layer and the surrounding fluid, where a turning point occurs indicating boundary-layer separation. Since the spreading layer is unstable, a secondary vortex forms in its place. The primary and secondary vortices continue their radial movement with opposite directions. After some time, they rebound from the impinging plate, creating a re-circulation zone near the impinging plate. For boundary-layer separation to occur, the negative pressure gradient of the vortex must be strong enough to overcome the impulse gradient in the boundary-layer. If this happens, separation and the formation of a secondary vortex occur, with measurements from various experiments indicating that this location exhibits a maximum in turbulence intensity.

When considering the heat transfer from a impinging plate to a jet, the axial distance of the impinging plate and whether the jet is excited or not are of great significance, as these are factors that determine the nature of heat transfer and the distribution of the Nusselt number. Generally, the heat transfer coefficient decreases as the jet moves radially away from its axis, thus the maximum Nusselt number occurs at the jet axis. If the axial distances are shorter, vortices are able to separate the boundary-layer at a radial distance of $r/D = 1$, leading to the appearance of a secondary vortex causing a local minimum in the heat transfer distribution. Furthermore, the primary and secondary vortices travel radially to deflect from the impinging plate at a distance of $r/D = 2$, resulting in a re-circulation zone of fluid that affects a new local maximum in heat transfer. At larger radial distances, heat transfer decreases. The fig. 1 will depict a visualization of vortex structures during the impingement of the jet on the impinging plate.

The dependence of the Nusselt number distribution on the Strouhal number is significant because acoustic excitations of the appropriate frequency influence the faster transition of turbulence, whereby the potential core shortens and the shearing layer grows and evolves more

rapidly. For this reason, the global maximum in heat transfer will occur in the case of an unperturbed jet at an axial distance from the impinging plate of L/D = 8-9, while in the case of a perturbed jet, it will occur at a distance of L/D = 5.

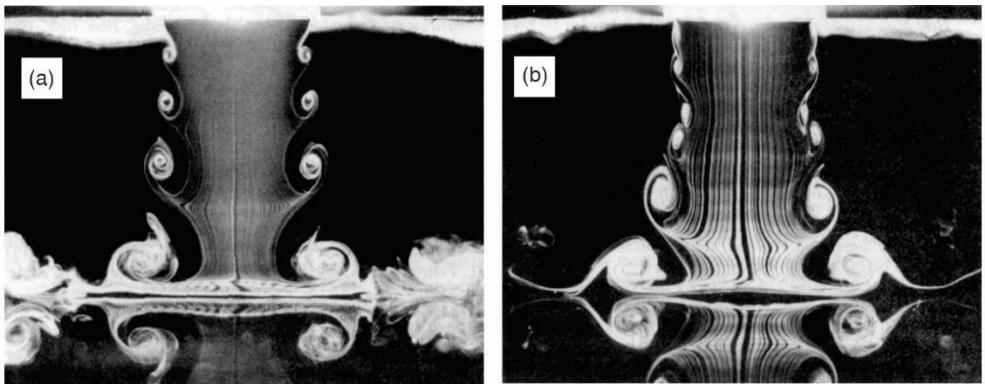

Figure 1. Visualization of vortex structures during the impingement of the jet on the impinging plate; (a) without pairing of vortices and (b) with pairing of vortices [8]

Numerical modelling

In order to numerically represent and better approximate the problem of jet impingement on a impinging plate, existing turbulent models implemented in software for simulations are used. These turbulent models often require modification [9-12] to be applied to the specific problem, as their primary structure relates to applications for flows parallel to the impinging plate, vortex traces, and similar phenomena. Therefore, changes to relevant terms and coefficients in the model equations are needed to apply them to the jet impingement problem, which is normally oriented. The flow characterized by such a jet is different because it first moves axially until it stops at the impinging plate, then turns and continues radially (parallel) to the impinging plate. In this work, mathematical modeling will not be pursued; instead, existing turbulent models within the ANSYS software framework will be applied, with results presented and compared to experimental data.

Due to all the differences compared to standard flows for which turbulent models were developed and the complexity of the flow field, even modified models will not provide exact results. However, the goal is to use them to enhance the original models and obtain more acceptable results in the stagnation zone region. This work will employ the standard k-ε model.

To solve the system of equations applied to the control volume using the mathematical model, certain assumptions need to be introduced, among which is the assumption that air will be considered as an incompressible fluid, but with temperature-dependent properties. In the numerical grid, the equation of continuity (1), RANS equation of motion (2), and the averaged energy equation (3) are solved:

$$\frac{\partial U_i}{\partial x_i} = 0 \tag{1}$$

$$\frac{\partial U_i}{\partial t} + U_i \frac{\partial U_j}{\partial x_j} = -\frac{1}{\rho}\frac{\partial P}{\partial x_i} + \frac{\partial}{\partial x_j}\left[\nu\left(\frac{\partial U_i}{\partial x_j} + \frac{\partial U_j}{\partial x_i}\right) - \overline{u_i u_j}\right] \tag{2}$$

$$\rho\frac{DT}{Dt}=\rho\frac{\partial T}{\partial t}+\rho U_j\frac{\partial T}{\partial x_j}=\frac{\partial}{\partial x_i}\left[\frac{\mu}{\mathrm{Pr}}\frac{\partial T}{\partial x_i}-\rho\overline{\theta u_i}\right] \tag{3}$$

Turbulent stress, based on the Boussinesq hypothesis, is a function of the local velocity gradient and the turbulent viscosity, μ_t, which is analogous to the relationship between viscous stresses and viscosity. In this way, a connection is established between the viscous stress tensor and the rate of strain tensor, as well as the turbulent stress tensor and the rate of strain tensor:

$$-\rho\overline{u_iu_j}=\tau_{ij}=\mu_t\left(\frac{\partial U_i}{\partial x_j}+\frac{\partial U_j}{\partial x_i}\right)=\mu_tS_{ij} \tag{4}$$

The method of calculating turbulent viscosity is defined by the mathematical model used to simulate turbulence. When the fluid moves along the impinging plate, there is stretching, so it is appropriate to use eq. (4). However, when it impacts the impinging plate, there is compression of fluid particles, and therefore terms related to compression deformation become dominant in the strain rate tensor. Therefore, if the impingement on the impinging plate is modeled as if it were shearing flow, the calculation leads to excessively high values of k (turbulent kinetic energy), increasing the turbulent viscosity, which later results in excessively high values of the Nusselt number. Moving away radially from the stagnation point, the calculations become more accurate because the flow becomes stretching, and the mathematical model accurately reflects the physics of the problem. The turbulent k-ε model consists of two transport eqs. (5) and (6), and the formula for calculating turbulent viscosity is also shown in (7):

$$\rho\frac{\partial k}{\partial t}+\rho U_i\frac{\partial k}{\partial x_i}=\frac{\partial}{\partial x_i}\left[\left(\mu+\frac{\mu_t}{\sigma_k}\right)\frac{\partial k}{\partial x_i}\right]+\mu_t\left(\frac{\partial U_i}{\partial x_j}+\frac{\partial U_j}{\partial x_i}\right)\frac{\partial U_i}{\partial x_j}-\rho\tilde{\varepsilon} \tag{5}$$

$$\rho\frac{\partial \varepsilon}{\partial t}+\rho U_i\frac{\partial \varepsilon}{\partial x_i}=\frac{\partial}{\partial x_i}\left[\left(\mu+\frac{\mu_t}{\sigma_\varepsilon}\right)\frac{\partial \varepsilon}{\partial x_i}\right]+f_1C_1\mu_t\frac{\varepsilon}{k}\left(\frac{\partial U_i}{\partial x_j}+\frac{\partial U_j}{\partial x_i}\right)\frac{\partial U_i}{\partial x_j}-\rho f_2C_2\frac{\varepsilon^2}{k}+E \tag{6}$$

$$\mu_t=\rho f_\mu C_\mu\frac{k^2}{\varepsilon} \tag{7}$$

In the previous differential partial equations, certain empirical constants, C_μ, C_1, C_2, σ_k, σ_ε, and damping functions, f_μ, f_1, f_2, are included for the accuracy of the model for flow near the wall. In eq. (5), the quantity $\tilde{\varepsilon}$ represents the current value of turbulent kinetic energy dissipation, for which there is a specific boundary condition.

Results and discussion

The simulations to be presented in this work can be divided into two types: those where the flow is observed as stationary, and those where it is variable in time. In the first case, there are no acoustic excitations, but the transfer of heat from the impinging plate to the jet is observed after assessing the velocity field of the fluid. In the non-stationary regime, acoustic excitations of different frequencies and amplitudes, which influence the modification of the fluid, are specified through the velocity profile at the inlet of the pipe nozzle, which varies sinusoidally with time. In this way, the influence of sound on the evolution of the jet and subsequent heat transfer is taken into account.

The application of computational fluid mechanics to the given problem was conducted using the software ANSYS FLUENT. Each numerical computation consists of several parts, which in this case were performed successively within the ANSYS *Workbench* framework. Initially, the geometry of the nozzle and the domain from which the fluid emerges were created. Subsequently, it was imported into *Workbench*, and the process of forming the numerical mesh was initiated. There are two types of meshes: unstructured and structured, and in this case, the decision was made to apply the former for both flow cases, as it yielded correct results. Since the version of ANSYS used was the student edition, the maximum number of mesh elements for computation was limited to 512000, which is not a particularly large value intended for demanding numerical computations.

The geometry was created in *Solidworks* by designing three separate parts: the first part representing the fluid domain where numerical analysis will be applied, while the other parts represent solid material, namely the nozzle wall and the impact surface. When imported into the initial stage of ANSYS *Workbench* within the *Geometry* section, an assembly is created consisting of the before mentioned parts. The key dimensions in this case are: the nozzle inner diameter is 25 mm, the thickness of the nozzle wall is 7.5 mm, the axial length of the nozzle is 150 mm, the axial distance from the nozzle exit to the impinging plate is 50 mm, the diameter of the impinging plate wall is 250 mm, and the thickness of the impinging plate wall is 10 mm. As can be observed, the problem is axisymmetric and 3-D. The axial length of the nozzle is set to 6*D* since a uniform velocity is imposed at its entrance to achieve a developed turbulent velocity profile along that straight section, which can be seen at outlet of nozzle when velocity contour is examined, due to the presence of a developed boundary-layer. The axial distance between the nozzle exit and the impinging plate is set to 2*D* as it is the most relevant aspect concerning vortex structures in the jet. The radial distance from the jet axis is set to 5*D* to capture the phenomenon of flow along the impinging plate and the interaction of the moving fluid with the stagnant surrounding. It should be noted that the nozzle inlet is labeled as inlet, the upper and outer parts of the cylindrical control volume are marked as outlet since the fluid is at rest there (surrounding environment). The designation wall represents the fluid walls as boundaries of the fluid domain, but it also applies to the walls of the solid domain, indicating their interaction.

An unstructured mesh was utilized, with tetrahedral elements selected. A higher mesh density was applied at locations of interest, namely the walls of the nozzle and impinging plate. To depict the boundary-layer effect occurring along the walls, the *Inflation* option was necessary. Thanks to this option, prism layers can be generated that exponentially increase with distance from the wall to capture the weakening of the viscosity effect.

The fig. 2 depicts the numerical mesh, which comprises 509929 elements, with mesh convergence achieved. Figure 3 provides a magnified view of the prism layers responsible for the boundary-layer.

The convergence of the computational mesh needed to be analyzed to select a mesh with an appropriate number of elements that yields accurate results (grid independent test). Three cases were compared, focusing on the maximum relative total pressure across the entire domain. The meshes contained 156754, 326358, and 509929 elements, respectively. The deviation in results between the first and second meshes was 3.024%, while the deviation between the second and third meshes was 0.857%. These findings indicate that increasing the number of elements significantly reduces result discrepancies. Since there is minimal difference between the second and third meshes, the second mesh could be considered adequate. However, given that ANSYS *Student* allows up to 512000 elements, and this is not computationally demanding, the densest mesh with 509929 elements was selected for the analysis.

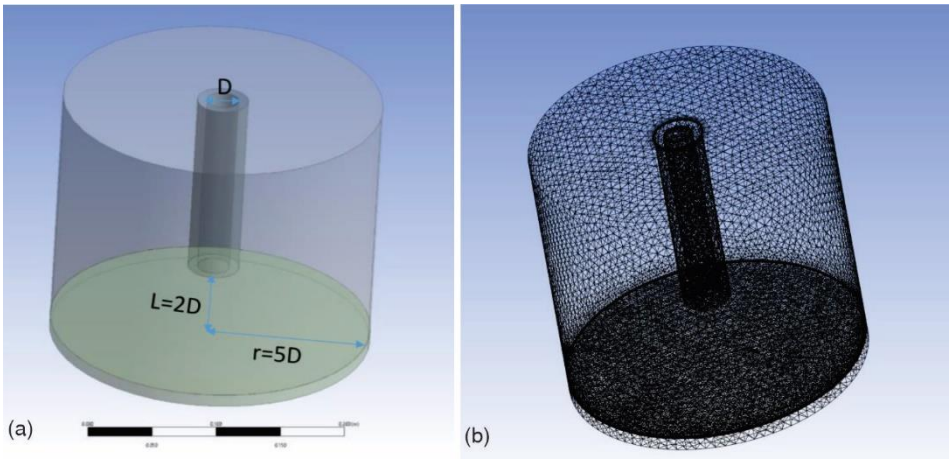

Figure 2. Geometry (a) and numerical mesh (b)

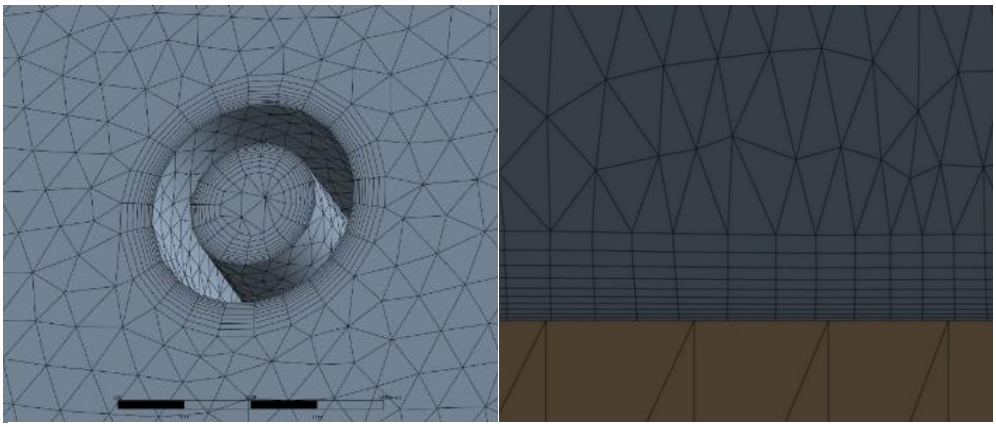

Figure 3. Using the *Inflation* option helps create prism segments near the wall to capture the boundary-layer effect better

Before starting the actual computations, it is necessary to select *Double Precision* and specify the number of processors involved in the calculation, which in this case is 4. Then, FLUENT is launched, where will be separately explained setting boundary conditions for stationary, non-stationary, and heat convection cases.

Stationary case

For the stationary case, the boundary conditions are set as: the inlet of the nozzle is labeled as *inlet*, where the velocity is specified. Based on the Reynolds number chosen to be Re = 10000, the velocity is calculated to be $U = 6.208$ m/s. This velocity is uniformly distributed across the entire inlet, and therefore, the length of the nozzle is set to 6D to ensure the formation of a developed turbulent profile at the nozzle exit. Recommended values are used for turbulence intensity and turbulent viscosity. As mentioned earlier, there are two outlets labeled as an *outlet*, where atmospheric pressure applies as they represent the calm air environment into which the jet flows. At locations where there is contact between solid and gas materials, such as the nozzle wall and impinging plate, the fluid-wall contact surface is designated as a *wall*. This implies

that such a boundary condition allows the wall to be stationary, non-slip, and have a certain roughness. Since there is interaction between the fluid and solid parts of the wall, they must be in contact. A convergence criterion of 10^{-6} is set, meaning that the calculation will strive to converge achieving that accuracy within a specified number of iterations, set at 1000. Then, in the *Initialization* tab, initial conditions are specified by selecting where the calculation starts, which in this case is the inlet of the nozzle.

Firstly, to visualize the results, a plane is created that intersects the domain along the axis of symmetry, resulting in a 2-D case showing the velocity distribution. In the subsequent figure, the development of the jet through the nozzle is observed, showing a developed turbulent profile upon exiting the nozzle. Upon contact between the wall and the fluid, a boundary-layer forms, which grows in the axial direction. Within the nozzle, there is a slight acceleration of the fluid, causing the air to exit the nozzle at a slightly higher velocity compared to its inlet velocity. As it starts to flow out, it encounters still air, leading to its expansion as depicted in the fig. 4. The velocity remains nearly unchanged within the potential core, which is short but remains unaffected by vortex influences, that do not grow sufficiently to penetrate into the jet axis. The shear layer occupies a larger space than the boundary-layer and contains vortices with a high negative pressure gradient, possessing sufficient velocity to overcome the impulse gradient in the boundary-layer along the impinging plate, leading to layer separation. In the stagnation zone, there is a sharp decrease in velocity as this is where the fluid directly impacts the impinging plate, resulting in maximal total pressure, influencing the fluid's redirection and subsequent radial movement along the impinging plate.

At a short radial distance from the jet axis, as observed on the impinging plate, there is an extreme value in velocity, followed by fluid deceleration until it completely stops at further distances. At a distance of 1*D* from the jet axis, the aforementioned phenomenon of boundary-layer separation occurs, accompanied by the formation of a secondary vortex, resulting in an increase in turbulence intensity, leading to the thickening of the shear layer on the impinging plate.

For the case of an axial distance of 0.01*D* from the impinging plate, the velocity profile in the boundary-layer is observed, and fig. 4 illustrates everything explained earlier in the text.

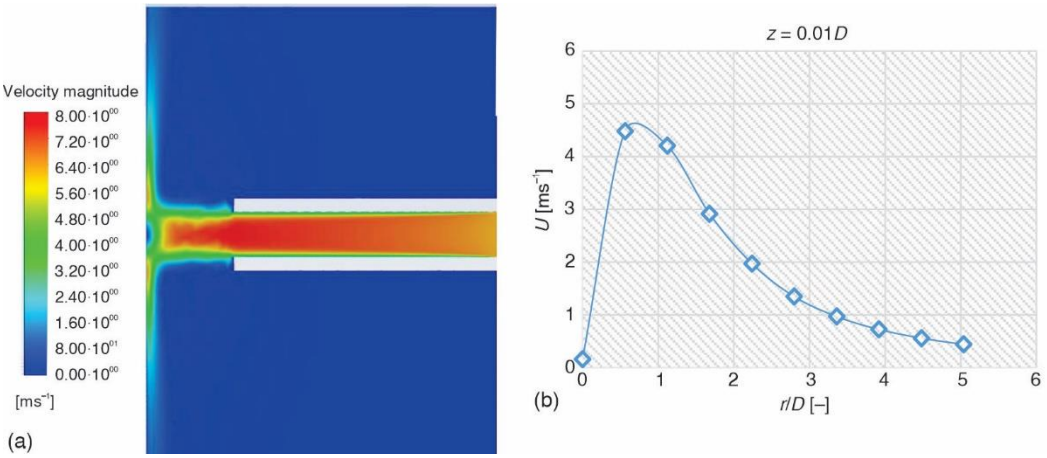

Figure 4. Velocity distribution upon jet impact on the impinging plate (a) and radial velocity profile for an axial distance of 0.01*D* (b) in an unperturbed jet

Table 1. Dependency of the Strouhal number value and the excitation frequency

S_t [–]	ω [Hz]
0.3	74.496
0.6	148.992
1	248.32
2	496.64

Unsteady case

In this type of experiment, another variable comes into consideration, namely time. Four cases of sound modifications with constant amplitude and unchanged Reynolds number will be observed regarding their effect on the velocity field. Sound stimulations are observed through the Strouhal number, which is varied for values of 0.3, 0.6, 1, and 2. Since the Reynolds number is the same as in the stationary regime and the diameter of the nozzle is known, the frequency corresponding to the given Strouhal number can be found, as shown in the tab. 1.

To represent the impact of sound excitations on the velocity at the inlet of the nozzle, the following equation is applied, which represents a sinusoidal variation of the initial velocity. Besides depending on the excitation frequency, it also depends on the amplitude, which is set to be 10% of the initial velocity:

$$U = U_0 + 0.1U_0 \sin(\omega t) \tag{8}$$

For this problem, it is desirable that within one-quarter period of the sinusoidal dependence of velocity on time, there are ten time intervals, whereby the time of one interval will be later utilized for *timestep*. The total number of intervals will be integral time over which the flow is observed.

Based on fig. 5, for each calculation, it can be seen separately how large the *timestep* should be. It is evident that with an increase in excitation frequency, the time interval required for simulation decreases, as shown in tab. 2.

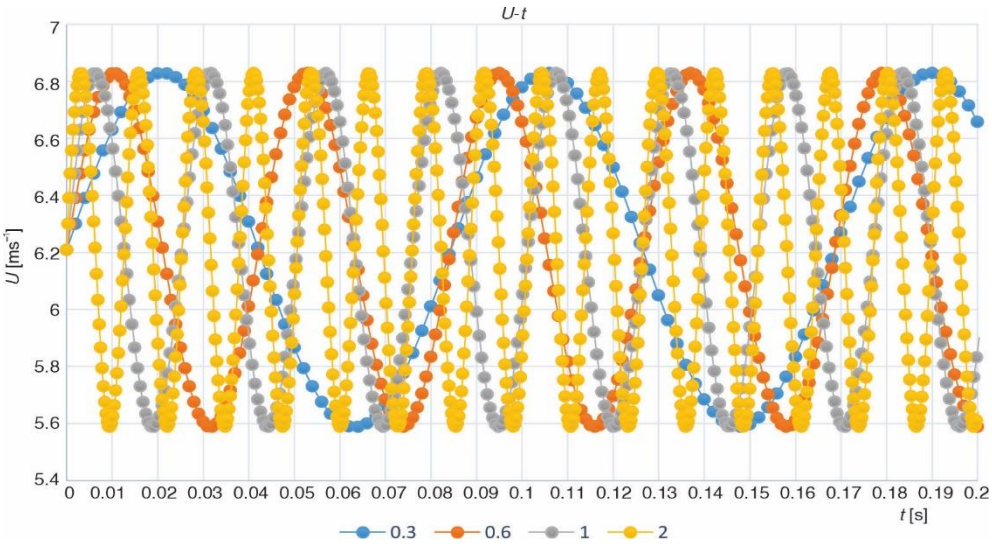

Figure 5. Dependency of the change in initial velocity over time due to the influence of sound with different frequencies (Strouhal numbers)

For all non-stationary calculations, the boundary conditions are the same as in the stationary case except at the inlet of the nozzle. Specifically, the change in inlet velocity over time under the influence of sound of a certain frequency and amplitude is applied through rela-

tion (8). The integral time for which the flow is observed is taken to be ten sinusoidal periods, which is actually 400 *timesteps*. The convergence criterion is set to be 10^{-5}. The number of iterations per time interval is taken to be 1000. The results for each investigated non-stationary flow will be successively displayed with an increase in the Strouhal number.

Table 2. Determination of the time interval for calculation based on the excitation frequency

S_t [–]	timestep [s]
0.3	0.0021
0.6	0.00105
1	0.00063
2	0.000315

The sound excitation when S_{tD} = 0.3 represents the desired mode of oscillation that influences the velocity modulation at the inlet of the nozzle, leading to a faster evolution of turbulence in the shear layer and a quicker transition of vortices, causing them to approach the impinging plate more slowly and not separate the boundary-layer as in the case without excitation. The velocity distribution and radial velocity profile in the boundary-layer for this excitation case are shown in the fig. 6.

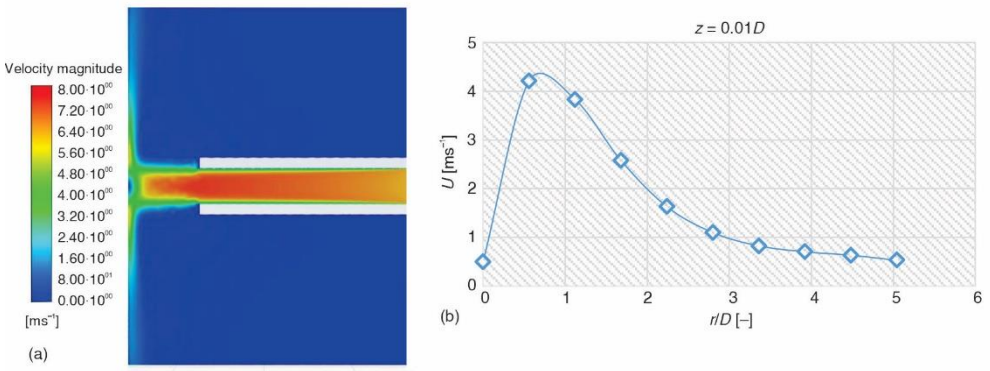

Figure 6. Velocity distribution upon jet impact on the impinging plate (a) and radial velocity profile for an axial distance of 0.01*D* (b) when S_{tD} = 0.3

In the case of excitation when S_{tD} = 0.6, it corresponds to vortex pairing in reality. Vortex pairing occurs at this frequency, where a stronger, higher-speed vortex is formed, subsequently leading to boundary-layer separation and the formation of a secondary vortex, with separation being less pronounced compared to the case without excitation, which is shown on fig. 7.

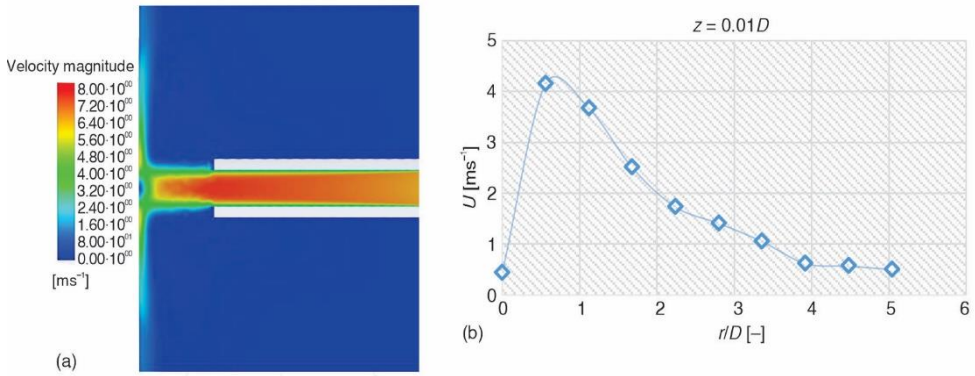

Figure 7. Velocity distribution upon jet impact on the impinging plate (a) and radial velocity profile for an axial distance of 0.01*D* (b) when S_{tD} = 0.6

In the case where S_{tD} = 1, fig. 8, in the velocity field depicted on the previous figure, a similar distribution is observed as in cases where the Strouhal number is equal to 0.3 and 0.6. When considering the velocity distribution in the boundary-layer, it is observed that the velocity peak is the highest compared to other excitations, indicating the largest separation of the boundary-layer, but stochastic changes in velocity are also observed at larger radial distances, indicating unpredictable behavior of vortices.

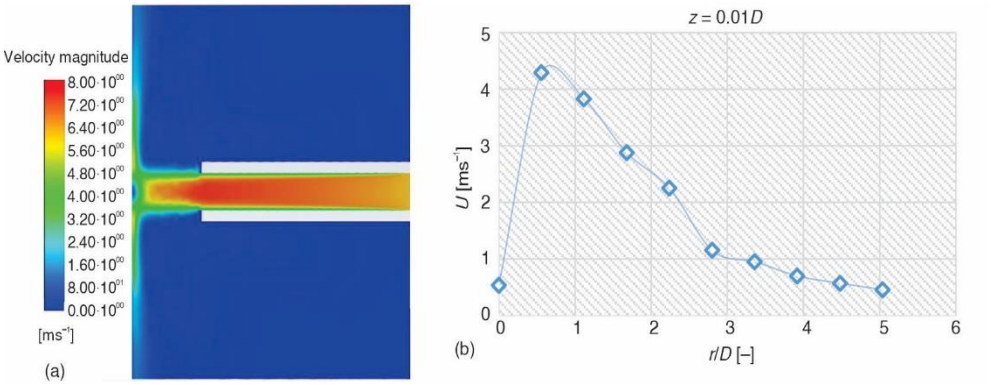

Figure 8. Velocity distribution upon jet impact on the impinging plate (a) and radial velocity profile for an axial distance of 0.01*D* (b) when S_{tD} = 1

When the excitation is such that S_{tD} = 2, fig. 9, it is observed that the potential core remains undisturbed and is larger than in previous cases because vortices under this excitation do not develop sufficiently to disrupt it. Otherwise, for this excitation mode, it is characteristic that the vortices are not fast enough to separate the boundary-layer from the impinging plate, but since the minimum axial distance is in this case, separation of the boundary-layer is possible. Interestingly, the velocity peak has higher values compared to other excitations due to the highest frequency, thus the fluid generally accelerates, but turbulence is not as pronounced as in earlier cases, rather the distributions are quite uniform. This is very significant because under this excitation, the best control of fluid-flow and heat transfer from the impinging plate to the jet is achieved, especially when considering the shortest axial distance.

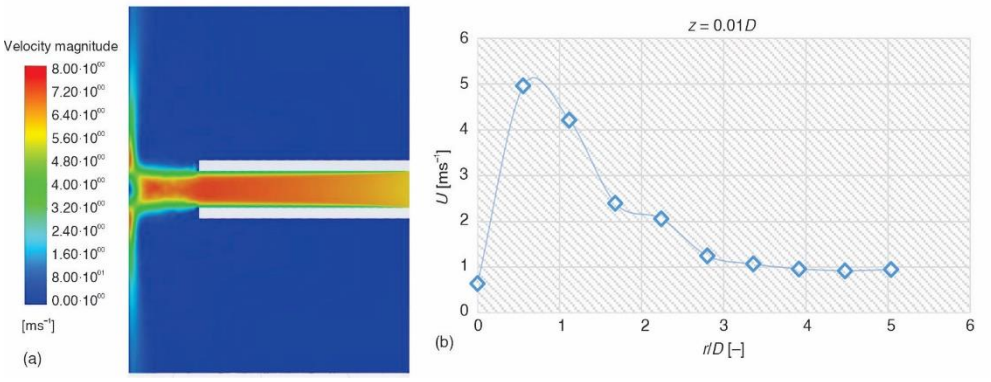

Figure 9. Velocity distribution upon jet impact on the impinging plate (a) and radial velocity profile for an axial distance of 0.01*D* (b) when S_{tD} = 2

Heat convection

In this section, the influence of vortex structures on the heat transfer from the heated surface to the air jet will be investigated for both unperturbed and perturbed cases of interest. To solve this issue in FLUENT, it is necessary to include the energy equation. Additionally, a boundary condition is set such that the temperature of the ambient air is 298.15 K. Only in the case of the ground wall, the heat flux heating this wall is chosen to be 1360 W/m^2. In cases without acoustic excitations, the convergence criterion for residuals is set to 10^{-6}, and the number of iterations is 1500. Regarding setting boundary conditions for cases involving sound and heat transfer, it is necessary to build upon the existing computation of the stationary regime, for which results have been obtained. For each excitation, a non-stationary case with an appropriate time interval and velocity change at the nozzle inlet, including the influence of heat, is applied individually. Non-stationary calculations are performed as described earlier, but since they are now appended to the stationary ones to achieve convergence, no initialization is required. The first output obtained from the results is the temperature field, from which the following quantities can be derived:

$$h = \frac{q}{T_\mathrm{w} - T_\mathrm{aw}} \tag{9}$$

$$\mathrm{Nu} = \frac{hD}{\lambda} \tag{10}$$

From the previous relations, it is evident that to obtain the heat transfer coefficient, it is necessary to know the heat flux, q, the change in temperature of the wall radially along the impinging plate, T_w, and the adiabatic wall temperature, T_aw, (room temperature, taken as 298.15 K). Subsequently, the Nusselt number distribution can be obtained, knowing the outlet diameter of the nozzle, as well as the thermal conductivity of air. The next figure will depict the dependency of Nu/(Re$^{7/10}$) and the radial distance from the axis of the jet. The Reynolds number is also taken into account for comparison with experimental results [6, 7], which will also be shown in the fig. 10.

The numerical results indicate that heat convection reaches its maximum near the axis of the jet, while there is a local minimum at the location of the secondary vortex formation upon boundary-layer separation, but also a local maximum when a re-circulation zone appears. At larger radial distances, there is a uniform decline in heat transfer. It can be concluded that there are no significant differences in heat transfer for both unperturbed and perturbed cases examined, especially at larger radial distances. More noticeable differences are observed in the stagnation zone, where the highest peak in heat transfer occurs for a perturbation when $S_{tD} = 2$, attributed to the highest fluid velocity in the boundary-layer.

When examining the experimental results, larger differences between perturbation cases are observed compared to what is depicted in the numerical simulations. Additionally, clear local minimums and maximums are evident at locations where secondary vortex and re-circulation zones occur, as well as at the axis of the jet and at the location of primary vortex influence, which is not the case with numerical results. The most significant changes in experiments are observed with unperturbed jets because that's where the greatest separation occurs, and the greatest uniformity of the convection profile is noticeable with a Strouhal number of 0.3, as at that point the vortices are most decelerated and a smaller secondary vortex is formed.

When comparing experimental and numerical results, fig. 10, it is evident that the numerical simulation has not captured the changes in convection accurately, presenting a much

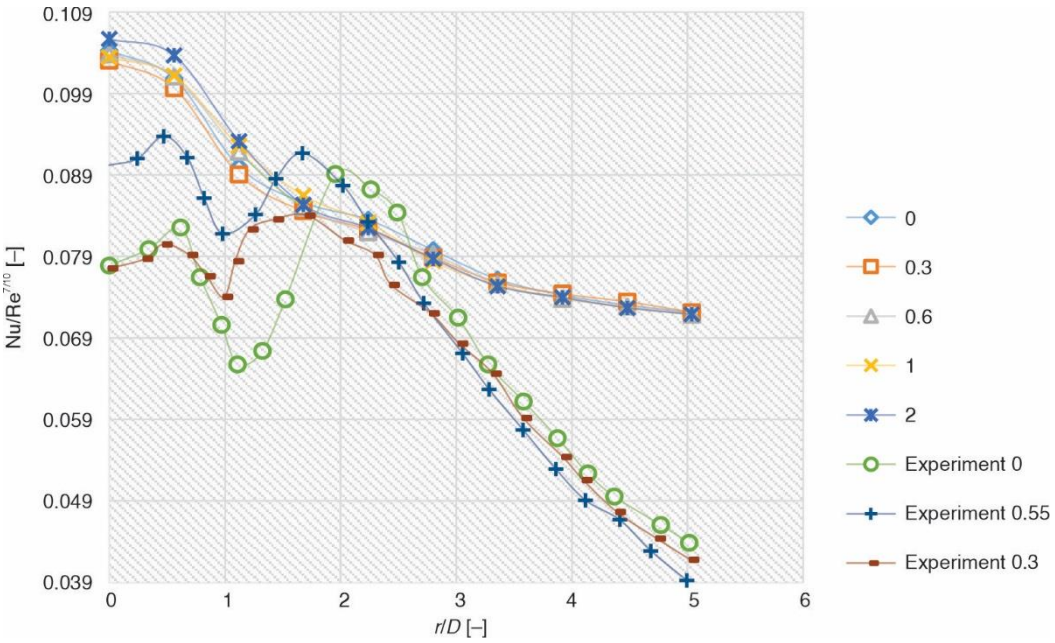

Figure 10. Heat transfer from the impinging plate to the jet at various Strouhal numbers and comparison with experimental data

more uniform profile than what occurs in reality. Additionally, it can be seen that the numerical results exceed the values most notably in the stagnation zone and at the domain periphery. Near the axis of the jet, numerical results are higher because normal stresses dominate there, while the mathematical model is formulated for tangential stresses. Since modifications of the k-ε model for low Reynolds turbulent numbers, which possess damping functions aimed at improving results in the stagnation zone and boundary-layer, were not utilized, such results are expected. At larger radial distances, the change in convection is much faster in experiments than in numerical simulations. The reason for this lies in the use of an unstructured mesh, where elements are equally distributed across the impinging plate. A structured mesh, which allows for the densest distribution in the stagnation zone and a gradual decrease in the number of elements towards the periphery, would certainly yield better agreement with experimental results.

Conclusions

In this study, the influence of acoustic modulations on the development of turbulent jets and vortices and their effect on the heat transfer from the impinging plate to the jet was investigated from a numerical perspective and the results were compared with corresponding experiments. These investigations are significant because for the shortest axial distance between the impinging plate and the nozzle, differences in jet behavior were found as a function of the type of excitation, especially in the velocity field, turbulence intensity and heat transfer. The highest value of the Nusselt number at the jet axis was determined for the excitation case with $S_{tD} = 2$, which can be attributed to the highest value of the Reynolds number in the boundary-layer at the impinging plate and the most uniform turbulence.

Finally, the experimental and numerical results were compared for cases where the Strouhal number for the thermal convection problem was equal to 0, 0.3, and 0.6. Differences were observed both in the stagnation zone and at the periphery of the domain. The reason for

the excess of the Nusselt number near the jet axis is that the standard k-ε model is formulated in such a way that shear stresses dominate over normal stresses in this region. Since no modifications of this model were used to partially mitigate the error by using damping functions, it is to be expected that such significant differences between the experiment and numerical simulation occur. Remarkable errors in the numerical calculation are also observed at the periphery due to the use of an unstructured grid. A structured grid would lead to a better agreement of the results since its elements would be distributed so that more of them are located in the stagnation zone and the number of elements gradually decreases with increasing radial distance from the jet axis.

Acknowledgment

This research was funded by the Ministry of Science, Technological Development and Innovation of the Republic of Serbia, Grant no. 451-03-136/2025-03/ 200017 ("Vinča" Institute of Nuclear Sciences, National Institute of the Republic of Serbia, University of Belgrade) and Science Fund of the Republic of Serbia - Green Program of Cooperation between Science and Industry - project STABILISE.

References

[1] Abramovich, G. N., *The Theory of Turbulent Jets*, English translation, M.I.T. Press, Cambridge, Mass., USA, 1963, pp. 671, https://doi.org/10.7551/mitpress/6781.001.0001
[2] Kataoka, K. *et al*, Unsteady Aspects of Large-Scale Coherent Structures and Impingement Heat Transfer in Round Air Jets With and Without Controlled Excitation, *Int. J. Engng Fluid Mech*, *25* (2005), 1, pp. 31-44
[3] Martin, H., Heat and Mass Transfer Between Impinging Gas Jets and Solid Surfaces, in: *Advances in Heat Transfer*, (eds.: Irvine Jr., T. F., Hartnett, J. P.), Academic Press, New York, USA, 1977, Vol. 13, pp. 1-60
[4] Stevanović, Ž., *Numerical Aspects of Turbulent Transfer of Momentum and Heat* (in Serbian), Publisher Grafika Galeb, Faculty of Mechanical Engineering, University of Niš, Nis, Serbia, 2008
[5] Ćetenović, N., Experimental and Numerical Analysis of the Influence of Acoustic Modulations of a Turbulent Air Jet on Heat Transfer from the Jet to the Surface (in Serbian), M. Sc. thesis, Faculty of Mechanical Engineering, University of Belgrade, Belgrade, 2023
[6] Cvetinović, D., Experimental and Numerical Investigation of the Influence of Turbulent Axisymmetric Jet Modification by Acoustic Oscillations on the Heat Transfer Process upon Impact on a Flat Heated Surface (in Serbian), Ph. D. thesis,, Faculty of Mechanical Engineering, University of Belgrade, Belgrade, 2014
[7] Cvetinović, D. *et al*, Velocity Measurements and Flow Structure Visualisations of a Self-Sustained Oscillating Jet, *Thermal Science*, *10* (2006), 2, pp. 113-125
[8] Popiel, C. O., Trass, O., Visualization of a Free and Impinging Round Jet, *Experimental Thermal and Fluid Science*, *4* (1991), 3, pp. 253-264
[9] Abid, R., Evaluation of Two-Equation Turbulence Models for Predicting Transitional Flows, *International Journal of Engineering Science*, *31* (1993), 6, pp. 831-840
[10] Baughn, J. W., *et al*., An Experimental Study of Entrainment Effect on the Heat Transfer from a Flat Surface to a Heated Circular Impinging jet, *J. Heat Transfer*, *113* (1991), 4, pp. 1023-1025
[11] Lam, C. K. G., Bremhost, K., A Modified Form of the k-ε Model for Prediction Wall Turbulence, *Transactions of the ASME, Journal of Fluids Engineering*, *103* (1981), 3, pp. 456-460
[12] Wang, S. J., Mujumdar, A. S., A Comparative Study of Five Low Reynolds Number k-ε Models for Impingement Heat Transfer, *Applied Thermal Engineering*, *25* (2005), 1, pp. 31-44

Paper submitted: October 30, 2024
Paper revised: November 27, 2024
Paper accepted: December 4, 2024